AIP | Journal of Applied Physics

The electronic and magnetic properties of La0.85Zr0.15MnO3 deposited on SrTiO3 and MgO substrates

N. G. Deshpande, C. H. Weng, Y. F. Wang, Y. C. Shao, C. Q. Cheng, D. C. Ling, H. C. Hsueh, C. H. Du, H. M. Tsai, C. W. Pao, H. J. Lin, J. F. Lee, J. W. Chiou, M. H. Tsai, and W. F. Pong

Citation: Journal of Applied Physics **115**, 233713 (2014); doi: 10.1063/1.4884230
View online: http://dx.doi.org/10.1063/1.4884230
View Table of Contents: http://scitation.aip.org/content/aip/journal/jap/115/23?ver=pdfcov
Published by the AIP Publishing

The electronic and magnetic properties of $La_{0.85}Zr_{0.15}MnO_3$ deposited on $SrTiO_3$ and MgO substrates

N. G. Deshpande,[1,2] C. H. Weng,[1] Y. F. Wang,[1] Y. C. Shao,[1] C. Q. Cheng,[1] D. C. Ling,[1,a)] H. C. Hsueh,[1] C. H. Du,[1] H. M. Tsai,[3] C. W. Pao,[3] H. J. Lin,[3] J. F. Lee,[3] J. W. Chiou,[4] M. H. Tsai,[5] and W. F. Pong[1,a)]
[1]*Department of Physics, Tamkang University, Tamsui 251, Taiwan*
[2]*Department of Physics, Shivaji University, Kolhapur-416004, Maharashtra, India*
[3]*National Synchrotron Radiation Research Center, Hsinchu 300, Taiwan*
[4]*Department of Applied Physics, National University of Kaohsiung, Kaohsiung 811, Taiwan*
[5]*Department of Physics, National Sun Yat-Sen University, Kaohsiung 804, Taiwan*

(Received 15 April 2014; accepted 7 June 2014; published online 19 June 2014)

The electronic and magnetic properties of tetravalent-ion-doped $La_{0.85}Zr_{0.15}MnO_3$ (LZMO) thin films that were epitaxially grown on $SrTiO_3$ (STO) and MgO substrates were studied using temperature-dependent x-ray diffraction (XRD), x-ray absorption near-edge structure, x-ray linear dichroism, and x-ray magnetic circular dichroism at the Mn $L_{3,2}$- and K-edge. XRD studies reveal that the LZMO thin films have compressive and tensile strains (along the ***c***-axis) on the STO and MgO substrates, respectively. As the temperature is reduced from room temperature to below magnetic transition temperature, the preferentially occupied Mn majority-spin e_g orbital changes from the in-plane $d_{x^2-y^2}$ to the out-of-plane $d_{3z^2-r^2}$ orbital for LZMO/STO, and vice versa for LZMO/MgO. Experimental results suggest that the new hopping path that is mediated by the Mn^{2+} ions triggers a stronger $d_{3z^2-r^2}$ orbital ordering of Mn^{3+} ions and enhances the ferromagnetic coupling between the Mn spin moments of t_{2g} electrons in LZMO/STO, whereas the strong tensile strain stabilizes the $d_{x^2-y^2}$ orbital by inducing lattice distortions of the MnO_6 octahedra in LZMO/MgO. [http://dx.doi.org/10.1063/1.4884230]

I. INTRODUCTION

Recently, colossal magnetoresistive perovskite manganites, $A_{1-x}B_xMnO_3$ (A = trivalent rare earth ions and B = divalent alkaline earth ions), have attracted considerable attention. These materials exhibit a remarkably rich variety of structural, magnetic, and transport properties[1–4] because of couplings between spin and orbital moments. Solovyev *et al.*[5] and Millis[6] argued that the magnetic properties of $A_{1-x}B_xMnO_3$ are determined by the competition between the anti-ferromagnetic (AFM) super-exchange of "t_{2g}" core spins and the ferromagnetic (FM) double-exchange (DE) of delocalized "e_g" electrons. The core electrons are relatively unaffected by the doping-induced strain,[7,8] oxygen stoichiometry,[9,10] or lattice mismatch.[11–13] However, structural distortions of the MnO_6 octahedra can change the electronic structures, which in turn modify the AFM and FM couplings between Mn spins.[13,14] Nanda and Satpathy showed that the lattice mismatch-induced epitaxial strain could cause an anisotropic hopping of electrons between orbitals and change spin orderings.[15] It is been also found that the current research is more focused on understanding the interfacial effects within the epitaxially grown perovskite-oxides thin films and different oriented substrates.[16–19] For instance, Garcia-Barriocanal *et al.*[18] experimentally observed the induced magnetic moment at the Ti sites in the $LaMnO_3/SrTiO_3$ (LMO/STO) epitaxial interface and attributed it to the formation of a new valence state of Ti^{3+} at the LMO/STO epitaxial interface by the transfer of charge from the Mn d-band to the empty conduction band of the titanate. To date, theoretical calculations and experimental studies have revealed that suitable doping or proper epitaxial strain can induce orbital ordering in single-crystalline or films of manganites.[11,12,20–22]

Many studies of hole-doped manganites have been performed, but studies of electron-doped manganites are fewer, probably because the radii of tetravalent electron-dopants differ greatly from those of the trivalent ions (specifically for "La"). In principle, tetravalent ion-doped LMO manganites can alter the electronic structure of the samples, enhancing the spin ordering of Mn ions and giving rise to a high Curie temperature. However, whether tetravalent dopants have the electron-doping effect in LMO compounds has not been conclusively determined.[23–25] Tetravalent dopants may behave like hole-dopants in LMO compounds.[26–30] Among tetravalent ion-doped LMO compounds, those doped with "Ce" have been the most extensively studied.[27,31] However, Ce doping has a few drawbacks: for example, Ce may exist in Ce^{3+} and Ce^{4+} valence states, changing the oxidation state of the Mn ions. Additionally, the $La_{1-x}Ce_xMnO_3$ samples are usually multiphase mixtures with CeO_2 inclusions.[32] In contrast, the "Zr" dopant has a single valence state of 4+ in $La_{1-x}Zr_xMnO_3$ manganite. Roy *et al.*[24] studied $La_{1-x}Zr_xMnO_3$ samples with various values of x (x = 0.05–0.2) and found that increasing the Zr content not only increases electrical conductivity but also enhances the hybridization between Mn d orbitals and O $2p$ states as well as the magnetic ordering. These results can

a)Authors to whom correspondence should be addressed. Electronic addresses: dcling@mail.tku.edu.tw and wfpong@mail.tku.edu.tw

be explained by the DE interaction through Mn^{2+}-O-Mn^{3+} and an increase of the Mn^{2+}/Mn^{3+} ratio. However, Wang *et al.*[33] investigated the transport properties of $La_{0.8}Zr_{0.2}MnO_3$ film and showed that the correlation between magnetic and transport properties is caused by the interaction between Mn^{3+} and Mn^{4+} ions rather than by the interaction between Mn^{2+} and Mn^{3+} ions. Therefore, whether the doping of Zr^{4+} into the LMO matrix generates an electron-doped and/or a hole-doped effect remains a matter of controversy. Multiple valence states of the Mn ions in $La_xMnO_{3-\delta}$ and $La_xSr_yMnO_3$ thin films have recently been identified,[34–36] suggesting unconventional charge transport in manganites. Hence, elucidating the underlying coupling mechanisms that govern the transport and magnetic properties of manganites will pave the way for developing new types of spintronic device.

In this study, x-ray diffraction (XRD) and x-ray absorption near-edge structure (XANES) measurements at the Mn *K*-edge and x-ray linear dichroism (XLD) and x-ray magnetic circular dichroism (XMCD) measurements at the Mn $L_{3,2}$-edge were performed at various temperatures to elucidate the atomic and electronic structures of epitaxially strained $La_{0.85}Zr_{0.15}MnO_3$ (LZMO) films. These measurements provide insight into the strain-induced preferential orbital occupation and spin character of the Mn ions in the samples of interest.

II. EXPERIMENTAL DETAILS

The crystal structures of the thin films were determined by using high-resolution XRD measurements at beamline-BL07 of the National Synchrotron Radiation Research Center (NSSRC), Hsinchu, Taiwan. X-ray energy was set to be 8 keV using a pair of Si (111) crystals and the beam size was controlled using a pair of slits (horizontal and vertical) in front of the sample. The experimental resolution was further improved by using a perfect crystal Ge (111) as the analyzer. The sample was glued on the cold head of a cryostat that was mounted on an 8-circle diffractometer, and then aligned with the incident photon by the Bragg reflections of the sample. XANES measurements at the Mn *K*-edge and XLD and XMCD measurements at the Mn $L_{3,2}$-edge were made at various temperatures in three beamlines (BL-17C, 11A, and 20A) at the NSSRC. Mn *K*-edge XANES spectra were obtained in total fluorescence yield mode, while Mn $L_{3,2}$-edge XANES/XLD/XMCD spectra were obtained in total electron yield mode. Mn $L_{3,2}$-edge XANES measurements were made at two angles of incidence (θ), (a) $\theta = 0°$-normal incidence (such that the electric field ***E*** of linearly polarized photons was parallel to the ***ab***–plane of the film), and (b) $\theta = 70°$-grazing incidence (with ***E*** almost parallel to the ***c***–axis of the film). The difference between the above two measurements is typically referred to as XLD, and helps to provide insight into the preferential occupation of the Mn majority-spin $3d$ e_g orbitals that is caused by the anisotropic effects related to various strains. The electrical resistivity and the magnetic properties were measured by the typical method using a four-point probe, a physical property measurement system, and a superconducting quantum interference device (SQUID) magnetometer, respectively. The bulk target of LZMO was prepared using the typical solid state reaction technique. La_2O_3, ZrO_2, and Mn_2O_3 powders with the La:Zr:Mn ratio of 0.85:0.15:1 were mixed in a mill for 1 h. The mixture was calcined in air at 900 °C and later heated for 1100 °C for 16 h. To make the target of this powder, it was pressed into pellets of an inch diameter and 0.6 cm thickness. Finally, it was sintered at 1238 °C in air for 12 h. The target sample was used in the deposition of LZMO thin films with a thickness of ~300 nm on STO and MgO (001) substrates by RF-sputtering. Post annealing of these as-deposited thin films in oxygen atmosphere for 30 min and 800 °C temperature was carried out in order to improve their crystallinity and to get ensured that the oxygen contents remain intact.

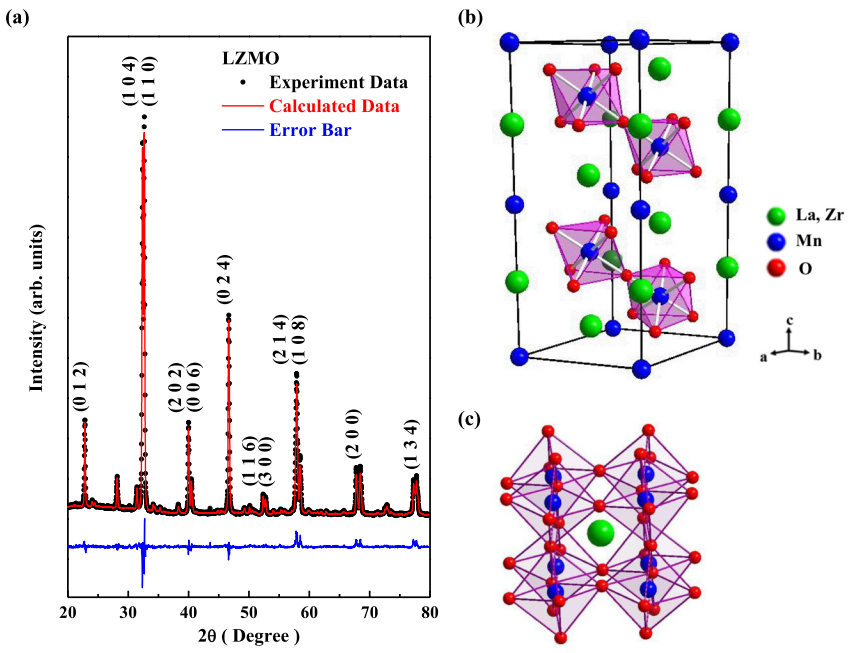

FIG. 1. (a) XRD pattern of bulk LZMO sample. Data are fitted using standard Rietveld technique. (b) and (c) Crystal structure of bulk LZMO with a rhombohedral lattice in space group *R*-3*C* and of the LZMO films deposited on STO and MgO substrates with an ABO_3 cubic lattice, respectively.

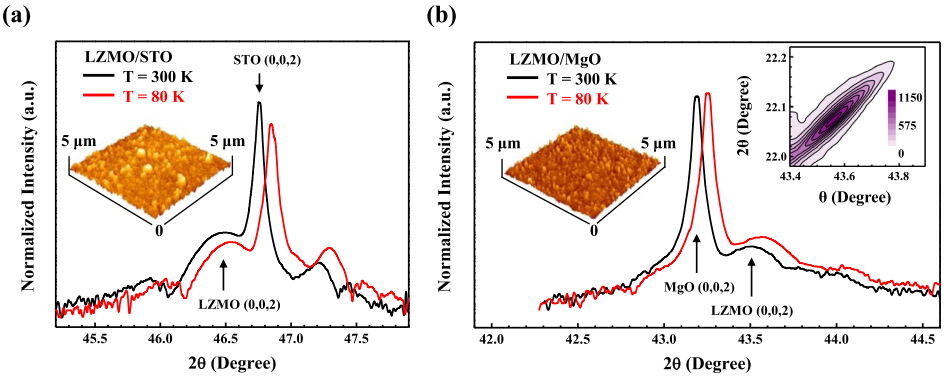

FIG. 2. High-resolution x-ray diffraction data for (a) LZMO/STO and (b) LZMO/MgO at T = 300 K and 80 K. Right-inset in (b) presents a mesh scan around (002), confirming reflection (002) from LZMO film on MgO substrate. Left-insets also present atomic force microscopic images of LZMO/STO and LZMO/MgO, respectively.

III. RESULTS AND DISCUSSION

The XRD pattern of the bulk LZMO sample reveals a rhombohedral structure with lattice parameters of $\boldsymbol{a} = \boldsymbol{b} = 5.523$ Å and $\boldsymbol{c} = 13.357$ Å, following refinement by the Rietveld technique [Figs. 1(a) and 1(b)].[37] A small peak appeared around 28°, which might be related to the ZrO_2 phase, indicating the difficulty in doping tetravalent-ion in $LaMnO_3$ matrix. Figures 2(a) and 2(b) present the high resolution XRD data through the Bragg peak (002) of the STO and MgO substrates, respectively, taken at T = 300 K and 80 K. Notably, in the following discussion of the XRD data and analysis, the pseudo-cubic notation is used for the thin films. The LZMO sample grown on the STO substrate, reflects weakly at approximately $2\theta = 46.505°$, and this reflection is indexed as the (002) reflection from LZMO with a pseudo-cubic cell.[38] With the lattice parameters of the substrate as a reference, the out-of-plane lattice mismatch of the LZMO film is calculated using $f = \frac{d_{sub}^{(002)} - d_{film}^{(002)}}{d_{sub}^{(002)}}$,[22,38,39] which yields $f = -0.512\%$, a compressive strain, for the STO substrate. XRD measurements were also made at T = 80 K [Fig. 2(a)]. The absence of any new reflection suggests that the crystal structure of LZMO remained intact even at 80 K. Figure 2(b) presents XRD measurements of the LZMO/MgO sample. In contrast, the reflection from the (002) plane of LZMO grown on STO substrate is at a lower angle than the main reflection from the Bragg peak (002) of STO in Fig. 2(a), a reflection at a higher angle ($2\theta = 43.509°$) than the main Bragg reflection from (002) of MgO ($2\theta = 43.187°$) is clearly seen. The strain was calculated and found to be $f = 0.689\%$, which represents a tensile strain. At T = 80 K, the crystalline structure of the LZMO film on MgO substrate also remained unchanged with tensile strain. Owing to the weakly reflecting nature of the LZMO film, a θ–2θ mesh-scan was performed [right-inset in Fig. 2(b)]; the reflection was confirmed. Accordingly, Table I presents the out-of-plane lattice parameter of the LZMO films grown on STO (001) and MgO (001), which is the ***c***-parameter of the pseudo-cubic unit cell, along with the calculated values of "*f*" at T = 300 K and 80 K. These results clearly indicate that the LZMO film exhibits compressive strain on the STO substrate and tensile strain on the MgO substrate at both 300 K and 80 K. Furthermore, the three-dimensional plots that were obtained from the atomic force microscopic images [left-insets in Figs. 2(a) and 2(b)] of the topography of the LZMO films on the two substrates reveal that grains in LZMO/MgO are smaller than those in LZMO/STO. The grain size is well known significantly to affect the magnetic and transport properties of the manganite thin films,[40] because the grain boundaries exhibit a short-range antiferromagnetic interaction and act as scattering sites.[24]

Figure 3 shows the temperature-dependence of resistivity and magnetization of the LZMO/STO, LZMO/MgO and bulk LZMO samples. From the figure, it is seen that the temperature-dependence of the resistivity of all of the samples exhibits a crossover from metallic behavior with $d\rho/dT > 0$ below T_{MI} to insulating behavior with $d\rho/dT < 0$ above T_{MI}, where T_{MI} denotes the metal-insulator transition temperature. The T_{MI} of the bulk LZMO sample was found

TABLE I. Comparison of lattice parameter, mismatch, and strain type of LZMO film grown on substrates of STO and MgO substrates at 300 K and 80 K.

LZMO/STO	300 K		80 K	
	STO (002)	LZMO (002)	STO (002)	LZMO (002)
2θ	46.753	46.505	46.846	46.530
Lattice parameter (Å)	3.906	3.926	3.899	3.924
Lattice mismatch, *f*	−0.512%		−0.641%	
Strain type	Compressive		Compressive	
LZMO/MgO	300 K		80 K	
	MgO (002)	LZMO (002)	MgO (002)	LZMO (002)
2θ	43.187	43.509	43.259	43.567
Lattice parameter (Å)	4.211	4.182	4.205	4.176
Lattice mismatch, *f*	0.689%		0.690%	
Strain type	Tensile		Tensile	

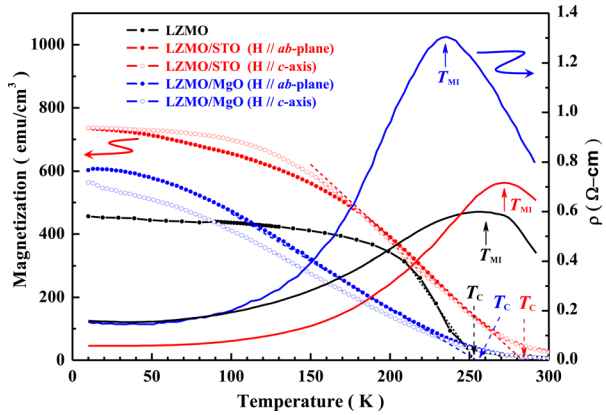

FIG. 3. Plot of temperature-dependence of resistivity and magnetization of the LZMO/STO, LZMO/MgO thin films and bulk LZMO samples. Note: Resistivity and magnetization measurements of the thin films were done along the sample *ab*-plane and the *c*-axis, respectively.

to be 260 ± 5 K, while those of LZMO/STO and LZMO/MgO were 270 ± 3 K and 230 ± 3 K, respectively. The fact that LZMO/STO has a slightly higher T_{MI} than that of the bulk sample, whereas LZMO/MgO has a substantially lower T_{MI} than that of the bulk LZMO sample will be discussed below. The resistivity of LZMO/STO is lower than that of LZMO/MgO in the temperature range 5–300 K, suggesting an enhancement of the charge transport of LZMO/STO that involves the higher number of delocalized Mn majority-spin e_g electrons.[41] The slope of the curve of the resistivity of LZMO/MgO around RT is much higher than that of LZMO/STO, indicating that a higher polaron hopping energy is required around RT.[42,43] This finding reveals that LZMO/MgO undergoes a strong local lattice distortion near RT. The above results together suggest that the substantial difference in T_{MI} and $d\rho/dT$ near RT between LZMO/STO and LZMO/MgO may arise from the relatively strong tensile strain in LZMO/MgO, as presented in Table I. Figure 3 also indicates the temperature-dependence of magnetization for all studied samples, all of which exhibit similar smooth ferromagnetic-to-paramagnetic transitions. The magnetic transition temperature, T_C, was determined by extrapolating the leading edge of the magnetization-versus-temperature curve to the baseline. The T_C of the bulk LZMO sample was found to be 252 ± 3 K, while those of LZMO/STO and LZMO/MgO were 285 ± 3 K and 255 ± 3 K, respectively. Clearly, the magnetization-versus-temperature curves in Fig. 3 indicate that the magnetization is consistently larger in LZMO/STO than in LZMO/MgO or the bulk LZMO sample over the range of temperatures considered. More interestingly, LZMO/STO and LZMO/MgO exhibit opposite magnetic anisotropy at/below T_C, the former has a larger magnetization along the ***c***-axis, while the latter has a larger magnetization in the ***ab***-plane. The opposite magnetic anisotropy can be related to the different preferential orbital occupancies of the highly directional Mn 3*d* orbitals in the distorted MnO_6 octahedra owing to a compressive strain in LZMO/STO and a tensile strain in LZMO/MgO. To evidently reconcile the above scenario and better understand the effect of strain on temperature-dependent resistivity and magnetization, the electronic and magnetic properties that are associated with the spin moment of the Mn ions in the LZMO/STO and LZMO/MgO samples were comprehensively studied as described below.

Figures 4(a) and 4(b) present the Mn $L_{3,2}$-edge XANES spectra of LZMO/STO and LZMO/MgO at two angles of incidence $\theta = 0°$ (with the electric field ***E*** parallel to the ***ab***-plane) and 70° (with the electric field ***E*** nearly parallel to the ***c***-axis) at temperatures of 80 K, 250 K, and RT, respectively. Corresponding spectra were obtained for the bulk LZMO, MnO, Mn_2O_3, and MnO_2 powder samples at angle $\theta = 0°$ at RT for reference. The spectra are primarily

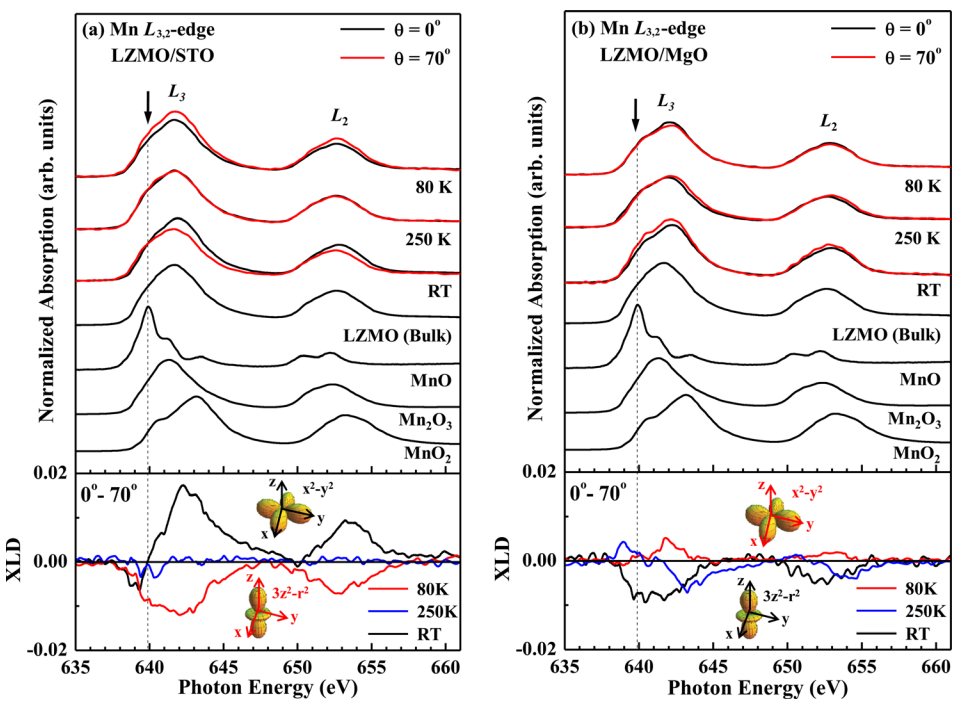

FIG. 4. (a) and (b) Normalized Mn $L_{3,2}$-edge XANES spectra of LZMO/STO and LZMO/MgO at two angles of incidence ($\theta = 0°$ and 70°), at temperatures 80 K, 250 K and RT. Results for bulk LZMO, MnO, Mn_2O_3, and MnO_2 are shown for reference. Bottom panels present corresponding XLD spectra. Schematic in-plane ($d_{x^2-y^2}$) and out-of-plane ($d_{3z^2-r^2}$) e_g orbitals are also displayed. Note: small flat plateau region indicated by an arrow/dotted line corresponds to MnO-like/Mn^{2+} valence state.

associated with the Mn $2p \rightarrow 3d$ transition, and the intensity of the main feature is attributable to the density of the unoccupied Mn 3*d*-O 2*p* hybridized states. The Mn $L_{3,2}$-edge XANES spectra shown in Figs. 4(a) and 4(b) include two features, an L_3-edge around 643 eV and an L_2-edge around 653 eV, separated by spin-orbit splitting. The broadening of these two features suggests multiple valence states of the Mn ions.[29] The Mn $L_{3,2}$–edge composes t_{2g} and e_g states owing to the crystal-field splitting. The general features at the Mn $L_{3,2}$-edge of LZMO/STO and LZMO/MgO are similar to those of bulk LZMO and the superposed spectra of Mn_2O_3 and MnO_2, with a large contribution from Mn_2O_3, indicative of the presence of both Mn^{3+} and Mn^{4+} states. Therefore, the most likely FM coupling in these samples involves Mn^{3+}/Mn^{4+} mixed valence states; this claim is in good agreement with those made elsewhere for tetravalent-ion hole-doped manganites.[28,29,33] Additionally, the spectra also show the MnO-like/Mn^{2+} state in LZMO/STO and LZMO/MgO, as evidenced by a plateau at approximately 640 eV indicated by an arrow/dotted line in Figs. 4(a) and 4(b), although this plateau was not very well resolved in the Mn L_3-edge XANES spectra. Another signature of the Mn^{2+} valence state in LZMO films was verified in the Mn *K*-edge XANES spectra at 80 K and RT at two angles of incidence $\theta = 0°$ and 70° in Figs. 5(a) and 5(b), which include three important features **A**, **B**, and **C**. The pre-edge features **A** to **B** below the main feature **C** arise from the Mn 1*s* transition into unoccupied Mn 3*d* and/or Mn 3*d*/4*p* hybridized states, which have *p* components that are projected at the Mn sites, as observed in many transition metal oxides.[44] The main feature **C** at the Mn *K*-edge corresponds to the high-energy Mn 4*p* states. To obtain a comprehensive understanding of the position of this feature, the insets in Figs. 5(a) and 5(b) present its derivative. If mainly Mn^{3+} and Mn^{4+} valence states were involved, the FM coupling in LZMO/STO and LZMO/MgO for which the Mn ions in these samples will be assigned to have a valence charge between +3 and +4. The thresholds of features will have higher energy than that of Mn_2O_3/Mn^{3+}, but have lower energy than that of MnO_2/Mn^{4+}. Clearly, the energy thresholds of the Mn *K*-edge features of the LZMO/STO, LZMO/MgO, and bulk LZMO samples are higher than that of MnO/Mn^{2+}, but are lower than that of MnO_2/Mn^{4+}, and nearly equal to that of Mn_2O_3/Mn^{3+}, at both $\theta = 0°$ and 70° as well as at temperatures 80 K and RT. Notably, the threshold energy of the features of LZMO/STO and LZMO/MgO is close to the mean of the features of MnO, Mn_2O_3, and MnO_2, as presented in Figs. 5(a) and 5(b). The above results clearly suggest that the LZMO/STO and LZMO/MgO samples contain Mn ions in multiple valence states of Mn ions (Mn^{3+}, Mn^{4+}, and Mn^{2+}). However, it is noteworthy to mention here that the dominant valence states of Mn ions are Mn^{3+} and Mn^{4+}; while Mn^{2+} is less abundant. For LZMO/STO, the intensity of the main feature at the Mn $L_{3,2}$-edge with the ***E*** field polarized in the ***ab***-plane ($\theta = 0°$) at RT is larger than that along the ***c***-axis ($\theta = 70°$); whereas for LZMO/MgO, the intensity is larger when the polarization of the ***E*** field is along the ***c***-axis ($\theta = 70°$), as shown in Figs. 4(a) and 4(b). The structural distortions that are caused by compressive or tensile strains are generally believed to tune the splitting of the crystal field and modulate the preferential orbital occupancy of the highly directional Mn 3*d* orbitals in the strained manganites.[21] Aruta *et al.* argued that Mn^{4+} ($3d^3$) and Mn^{2+} ($3d^5$) ions with high spin configuration are Jahn-Teller-inactive ions, which do not distort the octahedral symmetry. Therefore, these Mn ions are expected not to contribute significantly to the orbital anisotropy. Accordingly, only the effect of the Mn^{3+} ($3d^4$) ions on the orbital anisotropy should

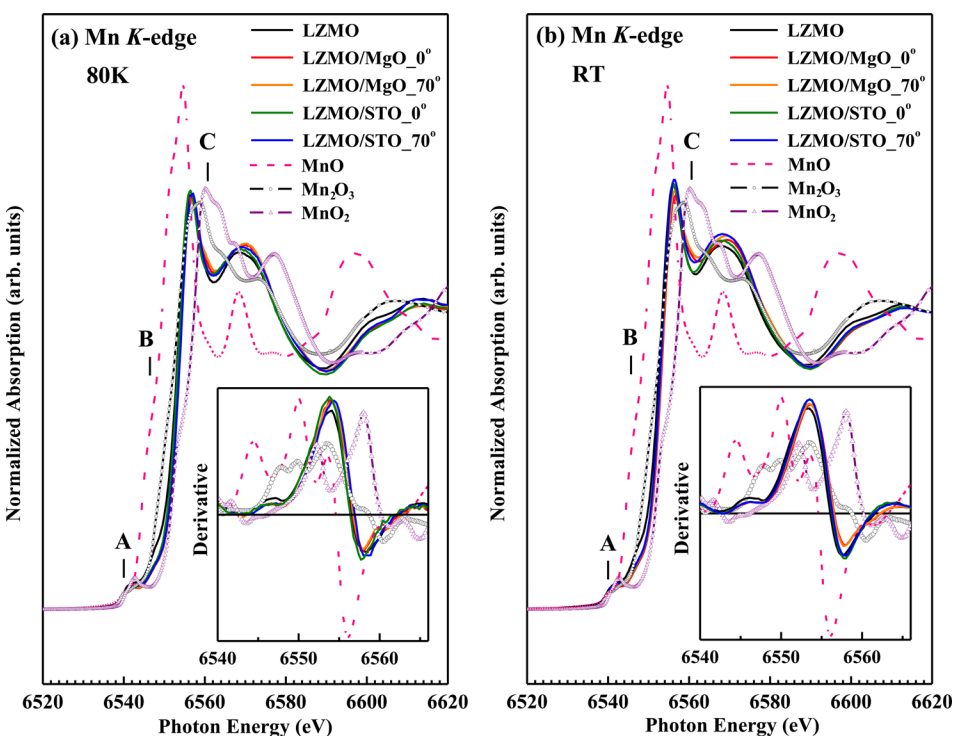

FIG. 5. (a) and (b) Mn *K*-edge XANES of LZMO/STO and LZMO/MgO at 80 K and RT at two angles of incidence $\theta = 0°$ and 70°. Mn *K*-edge XANES of reference bulk LZMO, MnO, Mn_2O_3, and MnO_2 powder samples at 80 K and RT at angle of incidence $\theta = 0°$ are shown for reference. Inset shown is the derivative of peak.

be taken into account in the analysis of the XLD spectra.[36] However, the sign, intensity, and line-shape of XLD is strongly dependent on the orbital ordering, which can be affected due to local distortion, crystal-field splitting, and anisotropic hopping integral.[45] In general, the line-shape of XLD can be altered for various MnO_6 octahedra systems, they are closely related to sample structural, chemical elements, composition[34] and strain,[46] so on. Importantly, it is worth to note that the sign of XLD integral intensity for similar local atomic structures should be consistent if they are preferable to have same orbital occupations.

Theoretical and experimental studies of the strained manganites have established that structural distortions of the unit cells are the major cause of the lowering of the energy of either the out-of-plane e_g orbital, $d_{3z^2-r^2}$, or the in-plane e_g orbital, $d_{x^2-y^2}$.[22,47,48] The bottom panels in Figs. 4(a) and 4(b) display the XLD spectra (between $\theta = 0°$ and 70°) at RT, 250 K, and 80 K, which are above, near, and below the transition temperatures of T_{MI} and T_C, respectively. These spectra provide information on the preferential Mn 3*d*-orbital occupancy under the influence of strains, due to the STO and MgO substrates. Clearly, the intensities of the XLD spectra of LZMO/STO greatly exceed those of LZMO/MgO at both RT and 80 K, consistent with the presence of more delocalized majority-spin e_g electrons in LZMO/STO, which was implied by resistivity measurements in Fig. 3. The sign of the XLD feature in the LZMO/STO spectrum is positive, suggesting that the in-plane Mn $d_{x^2-y^2}$ orbital is preferentially occupied by electrons at RT, while that of LZMO/MgO is negative, suggesting preferential occupation of the out-of-plane Mn $d_{3z^2-r^2}$ orbital at RT (above the transition temperatures). However, at 80 K (below the transition temperature), the signs of the XLD spectra are reversed. Close to the transition temperatures of T_{MI} and T_C, the XLD spectra of the samples at 250 K fluctuate between positive and negative values, suggesting that the two Mn majority-spin e_g orbitals are roughly equally occupied. The XLD results reveal that, for LZMO/STO, as the temperature is reduced from RT to less than the transition temperature of 80 K, the preferential occupancy of the majority-spin e_g orbitals changes from the in-plane $d_{x^2-y^2}$ to the out-of-plane $d_{3z^2-r^2}$; whereas for LZMO/MgO, the change is in the opposite direction. These experimental findings can be understood as being caused by the stabilization of the out-of-plane $3z^2$-r^2 (in-plane x^2-y^2) orbital that is induced by the compressive (tensile) strain that arises from a reduction of Coulomb repulsion interaction between Mn ions and O ligands.[36] This result can be associated with the magnetization anisotropy results in Fig. 3. Notably, similar strain- and temperature-induced changes in the sign of XLD intensity have been observed in $BiFeO_3$/$DyScO_3$ ($\boldsymbol{c/a} = 1.005$), $BiFeO_3$/$NdScO_3$ ($\boldsymbol{c/a} = 0.981$) thin films,[49] and $La_{0.6}Sr_{0.4}FeO_3$ film that is epitaxially grown on STO substrate below and above the Néel temperature.[50]

The top five panels of Figs. 6(a) and 6(b) present the Mn $L_{3,2}$-edge XANES spectra, with the photo-helicity of the incident x-rays parallel (μ_+) and anti-parallel (μ_-), respectively, to the direction of magnetization of the LZMO/STO and LZMO/MgO samples. These spectra were obtained at 80 K, 200 K, 230 K, 250 K, and RT at angle of incidence $\theta = 30°$ under an applied magnetic field of 1 Tesla parallel to the surface of the samples. The bottom panels of Figs. 6(a) and 6(b) present the Mn $L_{3,2}$-edge XMCD spectra, which reveal that both samples have the same FM phase below the transition temperature T_C. Although quantitative information concerning the spin and orbital moments of the Mn ions in the samples can be obtained principally by analyzing the XMCD curves using spin and orbital sum-rules,[51,52] the spin and orbital moments that are associated with the multiple valence states of Mn ions cannot be determined directly and accurately from the XMCD spectra by applying these sum-rules.[53] Therefore, the calculations made by applying the sum-rules to the XMCD spectra are not presented herein.

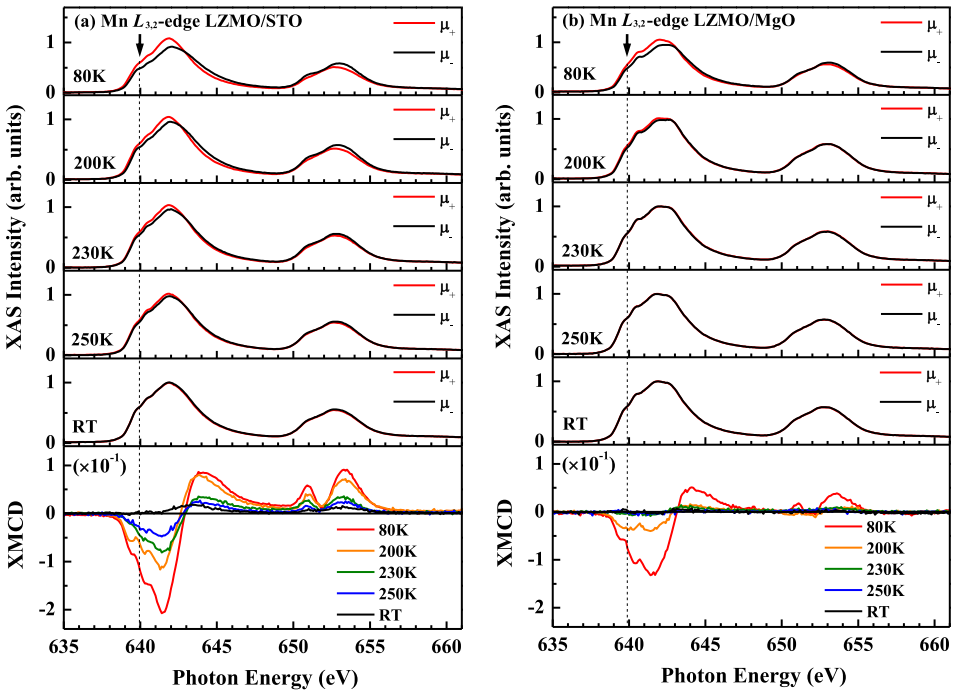

FIG. 6. (a) and (b) Normalized Mn $L_{3,2}$-edge XANES spectra of LZMO/STO and LZMO/MgO samples with photo-helicity of incident x-rays parallel (μ_+) and anti-parallel (μ_-) to direction of magnetization at various temperatures (80 K, 200 K, 230 K, 250 K, and RT) at angle of incidence $\theta = 30°$ in a magnetic field of 1 Tesla applied along the surface of the sample. Bottom panels display corresponding XMCD spectra. Note: the region indicated by an arrow/dotted line corresponds to MnO-like/Mn^{2+} valence state.

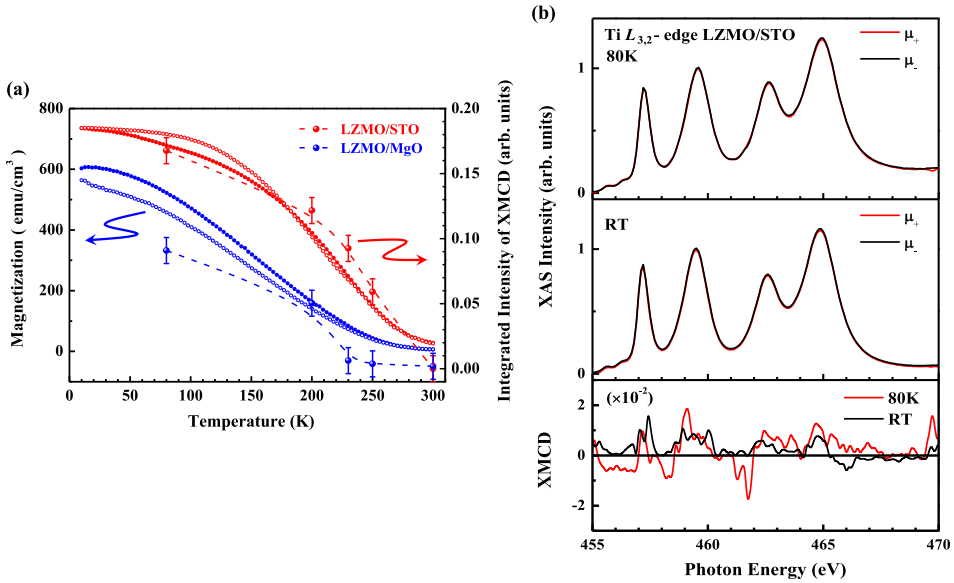

FIG. 7. (a) Comparison of integrated XMCD intensity and measured magnetization from Fig. 3. Dashed lines on XMCD data are guides for the eyes. (b) Ti $L_{3,2}$-edge XANES spectra with photo-helicity of incident x-rays parallel (μ_+) and anti-parallel (μ_-) to the direction of magnetization for LZMO/STO.

Nevertheless, the spin moment of the Mn ions can still be inferred from the intensity of XMCD and the general line-shape of the XMCD spectra. The integrated intensity of the XMCD feature (in the energy range 636–643 eV) at the Mn L_3-edge in LZMO/STO is approximately twice that of LZMO/MgO at/below T_C [see Fig. 7(a)]. Clearly, the greater XMCD intensity at the Mn $L_{3,2}$-edge observed in LZMO/STO is consistent with the larger magnetization observed in LZMO/STO in the ferromagnetic state, as shown in Fig. 3. The general features in the XMCD spectra in the bottom panels of Figs. 6(a) and 6(b) are quite similar to those of $La_xSr_{1-x}MnO_3$,[41,54] suggesting that Zr-dopant-induced delocalized majority-spin e_g electrons mediate the FM coupling and that the ferromagnetism is dominantly driven by the Mn^{3+}/Mn^{4+} DE mechanism. Additionally, the MnO-like/Mn^{2+} valence state contributes to the low-energy feature at ~640 eV more significantly below T_C than above T_C, as indicated by the arrow/dotted line in the XMCD spectra. Therefore, the bottom panels of Figs. 6(a) and 6(b) indicate that all the Mn_2O_3-like/Mn^{3+}, MnO_2-like/Mn^{4+}, and MnO-like/Mn^{2+} valence states contribute to the more intense XMCD spectrum of LZMO/STO than that of LZMO/MgO. Mn^{2+} ions have been considered to have a high-spin configuration, so they contribute to the strong magnetism in LZMO/STO, particularly below the transition temperature. These results suggest that a sample with a lower resistivity and a higher T_C has more Mn^{2+} valence states. Based on effective single-band model,[34] theoretical calculations show that a new hopping path for the DE mechanism, involving Mn^{2+} ions, Mn^{3+}-O^{2-}-Mn^{2+}-O^{2-}-Mn^{3+}, is energetically favorable in a distorted manganite when $d_{3z^2-r^2}$ orbitals of Mn^{3+} ions are preferentially occupied. In such a case, a significant overlap between the Mn 3*d* and O 2*p* orbitals in the out-of-plane direction considerably increases the overall hopping probability of delocalized e_g electrons and effectively strengthens the ferromagnetic coupling between localized t_{2g} electrons. Consequently, the manganite lattice contains a significant amount of Mn^{2+} ions, making it more metallic and increasing T_C with a larger magnetization. Recent experimental studies of nonstoichiometric $La_xMnO_{3-\delta}$ and $La_xSr_yMnO_3$ thin films have demonstrated the emergence of the new charge-hopping path through Mn^{2+} ions.[35,36] Since LZMO/STO contains more Mn^{2+} ions than does LZMO/MgO, the former has more delocalized majority-spin e_g electrons and, consequently, greater FM coupling and better transport properties. Figure 7(a) compares the integrated XMCD intensity with the magnetization measurements that are presented in Fig. 3. The variation of the integrated XMCD intensities with temperature below T_C for the LZMO/STO and LZMO/MgO samples is consistent with the general trend of the temperature-dependent magnetization, as displayed in Fig. 3. As the temperature is reduced, the magnetization is enhanced, as revealed by the increase in the XMCD intensity, which is consistent with the SQUID results.

Recently, Garcia-Barriocanal *et al.*[18] have found direct evidence of the effect of the interface on the magnetic properties of the LMO/STO epitaxial system. At the interface between titanate and manganite, the Mn-O-Ti bond may provide a means of interaction between the highly localized majority-spin t_{2g} electrons of Mn ions and the 3*d* electrons of Ti ions by delocalizing the Mn majority-spin e_g electrons. To understand the possible effect of charge transfer on the magnetic properties of LZMO/STO, Fig. 7(b) presents the Ti $L_{3,2}$-edge XANES spectra with the photo-helicity of the incident x-rays parallel (μ_+) and anti-parallel (μ_-) to the direction of magnetization. The figure also presents the XMCD spectra of LZMO/STO at 80 K and RT. The line-shapes in the XANES spectra at the Ti $L_{3,2}$-edge of LZMO/STO resemble those of the reference STO, reported elsewhere[54] strongly suggesting that the valence of the Ti ion in LZMO/STO is similar to that in STO at both 80 K and RT. Therefore, no evidence of a new valence state of the Ti ions, which would influence the observed ferromagnetism in LZMO/STO, was found and no clear XMCD signal is detected, as shown in the bottom panel of Fig. 7(b). Therefore, the fact that the magnetization is larger in LZMO/STO than in LZMO/MgO or the bulk LZMO sample follows mainly from the lattice-mismatch-induced epitaxial strains.

Notably, Fig. 7(a) involves two experimental techniques, measurement by SQUID and the determination of XMCD intensity at the Mn $L_{3,2}$-edge. Even though these two techniques have different characteristic probe depths, they reveal similar temperature-dependent magnetic properties of the LZMO/STO and LZMO/MgO samples, verifying the consistency of measurements.

IV. CONCLUSION

In summary, this investigation demonstrated that the LZMO thin films epitaxially grown on the STO and MgO substrates have compressive and tensile strain (along ***c***-axis), respectively, and behave more like a hole-doped system with Mn ions in Mn^{3+} and Mn^{4+} valence states. Also Mn^{2+} ions are present but in small amounts. As the temperature is decreased from RT to below T_C, for LZMO/STO, the preferential occupancy changes from the in-plane $d_{x^2-y^2}$ orbital to the out-of-plane $d_{3z^2-r^2}$ orbital; whereas for LZMO/MgO, the opposite change occurs. The new charge hopping mechanism that is activated by the Mn^{2+} ions is found to have an important role in a preferential occupation of the $d_{3z^2-r^2}$ orbital, and in the enhancement of T_C and conductivity, in LZMO/STO, whereas the strong tensile strain stabilizes the $d_{x^2-y^2}$ orbital by causing lattice distortions of the MnO_6 octahedra in LZMO/MgO. Therefore, one can tailor the electronic and magnetic properties of epitaxially grown LZMO thin films by simply using different substrates.

ACKNOWLEDGMENTS

The authors (D.C.L. and W.F.P.) would like to thank the National Science Council of Taiwan for financially supporting this research under Contract Nos. NSC 99-2112-M-032-004-MY3 and NSC 99-2119-M-032-004-MY3. N.G.D. is thankful to Department of Science and technology (DST), New Delhi for awarding DST INSPIRE Faculty award (IFA-13 PH-61).

[1]K. Chahara, T. Ohno, M. Kasai, and Y. Kozono, Appl. Phys. Lett. **63**, 1990 (1993).
[2]K. Khazeni, Y. X. Jia, L. Lu, V. H. Crespi, M. L. Cohen, and A. Zettl, Phys. Rev. Lett. **76**, 295 (1996).
[3]S. Jin, T. H. Tiefel, M. McCormack, R. A. Fastnacht, R. Ramesh, and L. H. Chen, Science **264**, 413 (1994).
[4]W. Zhang, A. Chen, F. Khatkhatay, C. F. Tsai, Q. Su, L. Jiao, X. Zhang, and H. Wang, ACS Appl. Mater. Interfaces **5**, 3995 (2013).
[5]I. Solovyev, N. Hamada, and K. Terakura, Phys. Rev. Lett. **76**, 4825 (1996).
[6]A. J. Millis, Phys. Rev. B **55**, 6405 (1997).
[7]Y. Moritomo, A. Asamitsu, and Y. Tokura, Phys. Rev. B **51**, 16491 (1995).
[8]A. Urushibara, Y. Moritomo, T. Arima, A. Asamitsu, G. Kido, and Y. Tokura, Phys. Rev. B **51**, 14103 (1995).
[9]J. F. Mitchell, D. N. Argyriou, C. D. Potter, D. G. Hinks, J. D. Jorgensen, and S. D. Bader, Phys. Rev. B **54**, 6172 (1996).
[10]K. M. Krishnan and H. L. Ju, Phys. Rev. B **60**, 14793 (1999).
[11]G. Colizzi, A. Filippetti, F. Cossu, and V. Fiorentini, Phys. Rev. B **78**, 235122 (2008).
[12]J. Zhang, H. Tanaka, T. Kanki, J. H. Choi, and T. Kawai, Phys. Rev. B **64**, 184404 (2001).
[13]T. Geng and N. Zhang, Phys. Lett. A **351**, 314 (2006).
[14]C. Ma, Z. Yang, and S. Picozzi, J. Phys.: Condens. Matter **18**, 7717 (2006).
[15]B. R. K. Nanda and S. Satpathy, Phys. Rev. B **78**, 054427 (2008).
[16]C. R. Ma, M. Liu, J. Liu, G. Collins, Y. M. Zhang, H. B. Wang, C. L. Chen, Y. Lin, J. He, J. C. Jiang, E. I. Meletis, and A. J. Jacobson, ACS Appl. Mater. Interfaces **6**, 2540 (2014).
[17]C. Ma, M. Liu, G. Collins, H. Wang, S. Bao, X. Xu, E. Enriquez, and C. Chen, ACS Appl. Mater. Interfaces **5**, 451 (2013).
[18]J. Garcia-Barriocanal, J. C. Cezar, F. Y. Bruno, P. Thakur, N. B. Brookes, C. Utfeld, A. Rivera-Calzada, S. R. Giblin, J. W. Taylor, J. A. Duffy, S. B. Dugdale, T. Nakamura, K. Kodama, C. Leon, S. Okamoto, and J. Santamaria, Nat. Commun. **1**, 82 (2010).
[19]M. Liu, C. Ma, J. Liu, G. Collins, C. Chen, J. He, J. Jiang, E. I. Meletis, L. Sun, A. J. Jacobson, and M. H. Whangbo, ACS Appl. Mater. Interfaces **4**, 5524 (2012).
[20]Y. Moritomo, Y. Tomioka, A. Asamitsu, Y. Tokura, and Y. Matsui, Phys. Rev. B **51**, 3297 (1995).
[21]D. J. Huang, W. B. Wu, G. Y. Guo, H. J. Lin, T. Y. Hou, C. F. Chang, C. T. Chen, A. Fujimori, T. Kimura, H. B. Huang, A. Tanaka, and T. Jo, Phys. Rev. Lett. **92**, 087202 (2004).
[22]C. Aruta, G. Ghiringhelli, A. Tebano, N. G. Boggio, N. B. Brookes, P. G. Medaglia, and G. Balestrino, Phys. Rev. B **73**, 235121 (2006).
[23]K. Asokan, J. C. Jan, K. V. R. Rao, J. W. Chiou, H. M. Tsai, S. Mookerjee, W. F. Pong, M.-H. Tsai, R. Kumar, S. Husain, and J. P. Srivastava, J. Phys.: Condens. Matter **16**, 3791 (2004).
[24]S. Roy and N. Ali, J. Appl. Phys. **89**, 7425 (2001).
[25]J. Gao, S. Y. Dai, and T. K. Li, Phys. Rev. B **67**, 153403 (2003).
[26]T. Yanagida, T. Kanki, B. Vilquin, H. Tanaka, and T. Kawai, J. Appl. Phys. **97**, 033905 (2005).
[27]T. Yanagida, T. Kanki, B. Vilquin, H. Tanaka, and T. Kawai, Phys. Rev. B **70**, 184437 (2004).
[28]P. Mandal and S. Das, Phys. Rev. B **56**, 15073 (1997).
[29]R. Werner, C. Raisch, V. Leca, V. Ion, S. Bals, G. V. Tendeloo, T. Chasse, R. Kleiner, and D. Koelle, Phys. Rev. B **79**, 054416 (2009).
[30]W. J. Chang, J. Y. Tsai, H.-T. Jeng, J.-Y. Lin, Kenneth Y.-J. Zhang, H. L. Liu, J. M. Lee, J. M. Chen, K. H. Wu, T. M. Uen, Y. S. Gou, and J. Y. Juang, Phys. Rev. B **72**, 132410 (2005).
[31]C. Mitra, Z. Hu, P. Raychaudhuri, S. Wirth, S. I. Csiszar, H. H. Hsieh, H.-J. Lin, C. T. Chen, and L. H. Tjeng, Phys. Rev. B **67**, 092404 (2003).
[32]R. Ganguly, I. K. Gopalakrishnan, and J. V. Yakhmi, J. Phys.: Condens. Matter **12**, L719 (2000).
[33]D. J. Wang, Y. W. Xie, B. G. Shen, and J. R. Sun, J. Phys.: Condens. Matter **18**, 741 (2006).
[34]P. Orgiani, A. Galdi, C. Aruta, V. Cataudella, G. De Filippis, C. A. Perroni, V. M. Ramaglia, R. Ciancio, N. B. Brookes, M. Moretti Sala, G. Ghiringhelli, and L. Maritato, Phys. Rev. B **82**, 205122 (2010).
[35]A. Galdi, C. Aruta, P. Orgiani, N. B. Brookes, G. Ghiringhelli, M. Moretti Sala, R. V. K. Mangalam, W. Prellier, U. Luders, and L. Maritato, Phys. Rev. B **83**, 064418 (2011).
[36]C. Aruta, M. Minola, A. Galdi, R. Ciancio, A. Yu. Petrov, N. B. Brookes, G. Ghiringhelli, L. Maritato, and P. Orgiani, Phys. Rev. B **86**, 115132 (2012).
[37]D. C. Ling, P. C. Hsu, and F. Z. Chien, J. Magn. Magn. Mater. **304**, e340 (2006).
[38]L. Malavasi, M. C. Mozzati, I. Alessandri, L. E. Depero, C. B. Azzoni, and G. Flor, J. Phys. Chem. B **108**, 13643 (2004).
[39]P. F. Fewster and C. J. Curling, J. Appl. Phys. **62**, 4154 (1987).
[40]G. Dezanneau, M. Audier, H. Vincent, C. Meneghini, and E. Djurado, Phys. Rev. B **69**, 014412 (2004).
[41]Y. Takamura, R. V. Chopdekar, E. Arenholz, and Y. Suzuki, Appl. Phys. Lett. **92**, 162504 (2008).
[42]A. Banerjee, S. Pal, E. Rozenberg, and B. K. Chaudhuri, J. Phys.: Condens. Matter **13**, 9489 (2001).
[43]P. Orgiani, C. Adamo, C. Barone, A. Galdi, A. Yu. Petrov, D. G. Schlom, and L. Maritato, Phys. Rev. B **76**, 012404 (2007).
[44]K. Asokan, Y. S. Chen, C. W. Pao, H. M. Tsai, C. W. Ou Lee, C. H. Lin, H. C. Hsueh, D. C. Ling, W. F. Pong, J. W. Choiu, M.-H. Tsai, and C. Moure, Appl. Phys. Lett. **95**, 131901 (2009).
[45]H. Wu, C. F. Chang, O. Schumann, Z. Hu, J. C. Cezar, T. Burnus, N. Hollmann, N. B. Brookes, A. Tanaka, M. Braden, L. H. Tjeng, and D. I. Khomskii, Phys. Rev. B **84**, 155126 (2011).
[46]A. Tebano, C. Aruta, S. Sanna, P. G. Medaglia, G. Balestrino, A. A. Sidorenko, R. De Renzi, G. Ghiringhelli, L. Braicovich, V. Bisogni, and N. B. Brookes, Phys. Rev. Lett. **100**, 137401 (2008).
[47]C. A. Perroni, V. Cataudella, G. De Filippis, G. Iadonisi, V. Marigliano, and F. Ventriglia, Phys. Rev. B **68**, 224424 (2003).

[48]C. Adamo, C. A. Perroni, V. Cataudella, G. De Filippis, P. Orgiani, and L. Maritato, Phys. Rev. B **79**, 045125 (2009).
[49]J. C. Yang, Q. He, S. J. Suresha, C. Y. Kuo, C. Y. Peng, R. C. Haislmaier, M. A. Motyka, G. Sheng, C. Adamo, H. J. Lin, Z. Hu, L. Chang, L. H. Tjeng, E. Arenholz, N. J. Podraza, M. Bernhagen, R. Uecker, D. G. Schlom, V. Gopalan, L. Q. Chen, C. T. Chen, R. Ramesh, and Y. H. Chu, Phys. Rev. Lett. **109**, 247606 (2012).
[50]D. Weller, J. Stöhr, R. Nakajima, A. Carl, M. G. Samant, C. Chappert, R. Mégy, P. Beauvillain, P. Veillet, and G. A. Held, Phys. Rev. Lett. **75**, 3752 (1995).
[51]B. T. Thole, P. Carra, F. Sette, and G. van der Laan, Phys. Rev. Lett. **68**, 1943 (1992).
[52]P. Carra, B. T. Thole, M. Altarelli, and X. D. Wang, Phys. Rev. Lett. **70**, 694 (1993).
[53]B. Y. Wang, H. T. Wang, S. B. Singh, Y. C. Shao, Y. F. Wang, C. H. Chuang, P. H. Yeh, J. W. Chiou, C. W. Pao, H. M. Tsai, H. J. Lin, J. F. Lee, C. Y. Tsai, W. F. Hsieh, M.-H. Tsai, and W. F. Pong, RSC Adv. **3**, 7884 (2013).
[54]F. Yang, M. Gu, E. Arenholz, N. D. Browning, and Y. Takamura, J. Appl. Phys. **111**, 013911 (2012).